JOURNAL OF AIRCRAFT
Vol. 46, No. 4, July–August 2009

Engineering Notes

Response Surface Technique for Static Aeroelastic Optimization on a High-Aspect-Ratio Wing

Guowei Yang,* Dawei Chen,* and Kai Cui*
Institute of Mechanics, Chinese Academy of Sciences, 100190 Beijing, People's Republic of China

DOI: 10.2514/1.42370

I. Introduction

IT IS a key subject in aircraft design to have the maximum lift and the minimum drag. Computational fluid dynamics (CFD)-based optimization design has been widely used to optimize rigid configurations in aircraft engineering [1,2]. As is well known, for a high-aspect-ratio wing, structural deformation can reduce its cruise aerodynamic performance. Because the aeroelastic characteristic has not been considered in the original optimum design, the real flight performances will deviate from the rigid-design results. Therefore, an optimum design that contains the aeroelastic effect needs to be developed. However, the static aeroelastic optimization is usually coupled with the aerodynamic model, structural model, optimization algorithms, and even such related issues as response surface method (RSM), fluid–structure interface, and moving grid. Therefore, it is much more difficult and time-consuming than the CFD aerodynamic optimization.

High-fidelity CFD tools are now available to aircraft designers and are commonly used in the design of aerodynamic configuration. CFD codes are capable of accurately predicting flowfields about complex aircraft configurations. Compared with linear aerodynamics, CFD tools are characterized by large computational costs due to complex geometrical modeling and grid generation. They require a higher level of proficiency from the users in defining run parameters and interpreting results.

Endeavors to exploit CFD solvers for aeroelastic analyses and aircraft structural design are relatively advanced, due to the main hindrance of large computational cost. They are typically characterized by iterations between CFD and a structure solver, which aggravate the problem of computational cost. Bennett and Edwards [3] reviewed the current state of computational aeroelasticity (CA), where CA is defined as the numerical analyses of coupled CFD and structural dynamics. They listed the main efforts needed in the development of CA: that is, the reduction of elapsed run times, improvement of the credibility of CFD tools, and simplification of methods for further applications. For the interface between fluid and structure, Smith et al. [4] provided a comprehensive review of spline methods, their mathematical formulation, and practical applications, which contain the infinite plate spline (IPS) for plate configuration and the beam spline for fuselage configuration. A large amount of literature exists on the subject of grid deformation, which mainly contains the algebraic transfinite interpolation (TFI) [5], the spring-network analogy by Batina [6] and Farhat et al. [7], and the boundary element method by Chen and Hill [8].

Even fluid–structure multidisciplinary optimization may cut down the design cycles and reduce the reliance on wind-tunnel and flight tests; the drawbacks are the repeated fluid–structure coupling analyses during the optimization process. At present, there are very few studies that consider the adaptation of CFD-based aeroelastic analyses in structural-design optimization. Applications of CFD-based structural and multidisciplinary design optimization were reviewed by Guruswamy and Obayashi [9]. Martins et al. [10–12] presented a CFD-based methodology for aerodynamic-structural optimization. Cross sensitivity is computed by the adjoint method, which was shown to be vastly more computationally efficient for a supersonic business jet optimization involving a larger number of design variables than ever. Reuther et al. [13] presented a structural optimization in which the aerodynamic and structural analyses were performed separately. CFD analyses were used to generate a response surface, and the response surface was incorporated in the structural optimization to improve the roll maneuverability, in which only the generation of a response surface required an amount of CFD-based analyses.

In this Note, a quadratic polynomial response surface model is put forward based on the CFD-based static aeroelastic calculations. The structure is represented by a finite element model and holds fixed in the optimization process. The genetic algorithm (GA) optimization method is used for the improvement of static aeroelastic performance through the optimization of the spanwise sectional airfoil shapes. To reduce the amount of CFD-based static aeroelastic analyses for the generation of RSM, only two sectional airfoils are chosen for the optimizations. Either for single- or multi-objectives optimizations, the study shows that the optimization of aeroelastic performances can be greatly improved compared with the original static aeroelastic results.

II. Static Aeroelastic Computational Methods

A. CFD Method

Fluid dynamic equations are the unsteady three-dimensional Navier–Stokes equations in strong conservation-law form. The inviscid terms are approximated by the modified third-order upwind Harten–Lax–van Leer–Einfeldt–Wada (HLLEW) schemes of Obayashi and Guruswamy [14]. For the isentropic flow, the scheme results in the standard upwind-based flux-difference-splitting scheme of Roe, and as the jump in entropy becomes large in the flow, the scheme turns into the standard HLLEW scheme. The viscous terms are discretized by the second-order central difference. The multiblock structured-grid-based Navier–Stokes solver [15] originally developed by the authors involves several turbulent models, and only the Baldwin–Lomax turbulence model is used in this Note. The lower/upper symmetric Gauss–Seidel method is used for the temporal discretization.

B. Computational Structural Mechanics Method

MSC Nastran software was used for the construction of the finite element structural model. The structural stiffness matrix is assumed to be unchangeable under the optimization process. The structural static equation is

$$q_s = [K]^{-1} F_s \tag{1}$$

where q_s represents the structural deformation, $[K]$ is the structural stiffness matrix, and F_s is the aerodynamic force on the structural grid points. For the complex aircraft configurations, the subzone interpolations need to be applied.

Received 4 December 2008; revision received 12 March 2009; accepted for publication 15 March 2009.

*Professor, Key Laboratory of High Temperature Gas Dynamics; gwyang@imech.ac.cn.

C. Data Transfer

After Eq. (1) is solved, the deformations on the structural grid points are known. The IPS method is used to interpolate the deformations to the aerodynamic surface grid points. The linear displacement transformation can be written in the form

$$q_a = [G]q_s \tag{2}$$

where q_a is the displacement on the aerodynamic grid points, and $[G]$ is the transformation matrix. The force transformation from the structural grid points to fluid grid points can be represented with the principle of virtual work as

$$F_s = [G]^T F_a \tag{3}$$

where F_a represents the aerodynamic forces on the fluid-surface grid points. The principle of virtual work can guarantee the conservation of energy between the fluid and structural systems.

In the practical application, the lower/upper decompositions of the transfer matrix $[G]$ and $[G]^T$ are precalculated and stored, which are unchangeable in the whole computational process.

D. Grid Deformation

For an aircraft configuration, a multiblock structured grid can be generated with Gridgen or other software. After the fluid-surface grid deformation is known from Eq. (2), the spring-network method and the TFI method are applied to deform the multiblock grid. The spring-network method is only used to get the deformation of multiblock boundary points, and one-, two-, and three-dimensional TFI methods are interpolated using the deformation values of edges, surface, and inner grid of each block. For the small and moderate aeroelastic deformations, the method can maintain the quality of the original grid and maximizes the reusability of the original grid.

E. Static Aeroelastic Solving Process

First, the steady flowfields are calculated with the fluid governing equations. Second, the loads on the aerodynamic surface grid center points are computed and interpolated to the structural grid points by Eq. (3). Third, the structural deformations are solved by Eq. (1). Fourth, the deformation values are interpolated to the aerodynamic surface grid points by Eq. (2). Fifth, the new grid is generated by the grid deformation method. Then the whole process can be repeated again until the structural configuration keeps unchangeable.

III. Optimization Algorithms

A. RSM Method

The RSM used in this Note is the quadratic polynomial model [16]. A set of samples based on CFD-based static aeroelastic calculations is used for the modeling of the RSM. Once the model has been established, the static aeroelastic performance of the aircraft configuration can be obtained, with the polynomial model for the design variables of the wing. Very little time is needed compared with the direct optimization process, in which CFD-based static aeroelastic solver is repeatedly employed. The RSM model is shown next as

$$y = \beta_0 + \sum_{j=1}^{k} \beta_j x_j + \sum_{j=1}^{k} \beta_{jj} x_j^2 + \sum_{i=1}^{k-1} \sum_{j=i+1}^{k} \beta_{ij} x_i x_j \tag{4}$$

where y represents the responses of the static aeroelastic aerodynamic performances such as lift and (or) drag coefficients, and x represents the normalized design variables, where

$$x_i = \hat{x}_i \frac{(\hat{x}_{\max_i} - \hat{x}_{\min_i})}{2} + \frac{(\hat{x}_{\max_i} + \hat{x}_{\min_i})}{2} \tag{5}$$

and where $\hat{x}_i$ are the original design variables, $\hat{x}_{\max_i}$ and $\hat{x}_{\min_i}$ are the maximum and minimum number of $\hat{x}_i$, k is the number of the design variables, and β are the coefficients of the RSM model that need to be determined. At least $K = (k+1)(k+2)/2$ samples have to be known, which required an excessive amount of CFD-based static aeroelastic calculations with a large number of design variables.

For n samples, the RSM model can be written in matrix form:

$$y = X \cdot a, \qquad y = \begin{Bmatrix} y_1 \\ y_2 \\ \vdots \\ y_n \end{Bmatrix}, \qquad X = \begin{Bmatrix} 1 & x_{11} & x_{12} & \cdots & x_{1k} \\ 1 & x_{21} & x_{22} & \cdots & x_{2k} \\ \vdots & \vdots & \vdots & \vdots & \vdots \\ 1 & x_{n1} & x_{n2} & \cdots & x_{nk} \end{Bmatrix}$$
$$a = \begin{Bmatrix} \beta_0 \\ \beta_1 \\ \vdots \\ \beta_k \end{Bmatrix} \tag{6}$$

The coefficients set a can be determined with the method of least squares:

$$b = (X^T X)^{-1} X^T y \tag{7}$$

The result can be evaluated by R^2 and R_a^2. The closer R^2 and R_a^2 approach 1, the more precise the RSM model. R^2 and R_a^2 can be expressed as

$$R^2 = 1 - \frac{SS_E}{SS_T}, \qquad R_a^2 = 1 - \frac{SS_E/(n-k-1)}{SS_T/(n-1)}$$
$$SS_E = (y^T y - a^T X^T y), \qquad SS_T = y^T y - \frac{1}{n}\sum_{i=1}^{n} y_i \tag{8}$$

B. Genetic Algorithm

In this Note, the real-coded adaptive-range genetic algorithms (ARGAs) proposed by Arakawa and Hagiwara [17] are used for single- and multi-objective optimizations. The ARGAs adapt the popularization to promising design regions during the optimization process and enable efficient and robust search for good precision while keeping the string length small. In ARGAs, the real-value design variable x_i is rewritten in terms of a real number r_i in [0,1], which is defined by an integral of Gaussian function from $-\infty$ to x_{ni}:

$$r_i = \int_{-\infty}^{x_{ni}} N(0,1)(z)\mathrm{d}z \tag{9}$$

$$x_i = \sigma \cdot x_{ni} + \propto \tag{10}$$

The mean value $\propto$ and the standard deviation σ of each design variable are calculated by the top half of the present population. To prevent inconsistency between the actual and updated population statistics, $\propto$ and σ are updated every N generations (taken as $N = 4$ in this Note) and then the population is reinitialized. To improve robustness of the present ARGAs, the following relaxation is also introduced to update the mean values $\propto$ and standard deviation σ:

$$\propto_{\text{new}} = \propto_{\text{present}} + \omega_{\propto}(\propto_{\text{sampling}} - \propto_{\text{present}}) \tag{11}$$

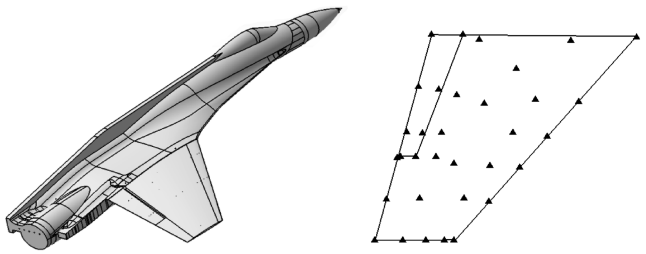

a) Static aeroelastic experimental model b) Flexible structural model

Fig. 1 Illustrations of a) static aeroelastic experimental model and b) flexible structural model.

$$\sigma_{\text{new}} = \sigma_{\text{present}} + \omega_\sigma(\sigma_{\text{sampling}} - \sigma_{\text{present}}) \tag{12}$$

where ω_α and ω_σ are the relaxation factors in [0,1] (taken as 1 and 0.5 in this Note, respectively), and α_{sampling} and σ_{sampling} are determined by sampling the top half of the present population. Other techniques in the ARGAs include the elitist strategy (the best and the second-best individuals are copied into the next generation), parental selection by stochastic universal sampling with ranking using Michalewicz's nonlinear function, and crossover and mutation with adaptive probabilities.

C. Multi-Objective Pareto Solution

Although single-objective optimization problems may have a unique optimal solution, multi-objective optimization problems often present a set of compromised solutions, known as the Pareto-optimal solutions, which are optimal in the sense that no other solutions in the search space are superior to them when all objectives

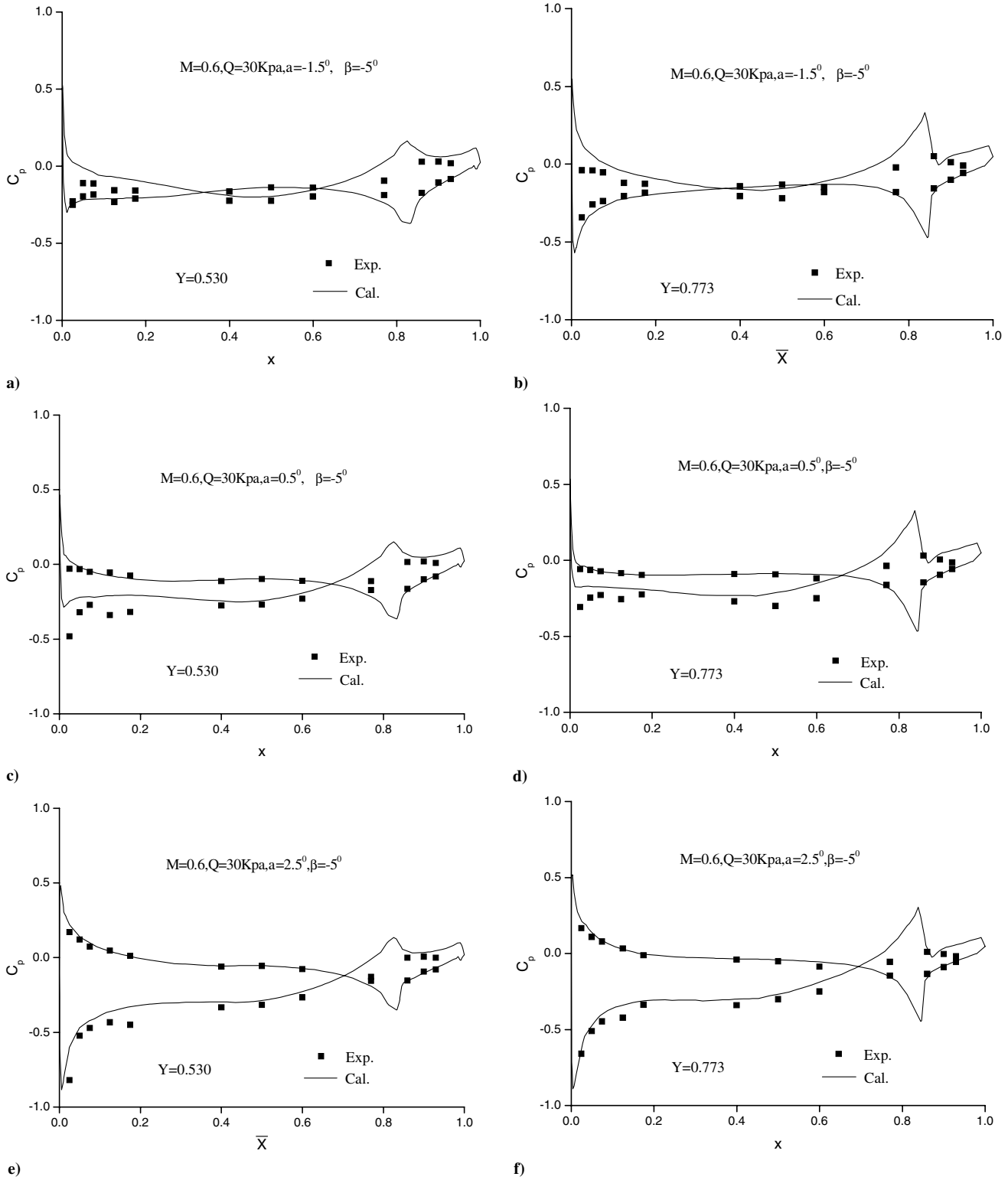

Fig. 2 Comparison of static aeroelastic computational pressure distributions with experiments.

are considered. In general, the goal is to find as many Pareto-optimal solutions as possible. In this Note, the Pareto-based multi-objective genetic algorithms given by Goldberg [18] are used.

For the minimum multi-objective problem, minimize $f_1(x)$, $f_2(x), \ldots, f_m(x)$ and any two individuals of l and k, then f_i^l and f_i^k are chosen to be the ith objective. Set up a two-dimensional matrix $R = [r_{ik}]_{N\cdot N}$, and define $v_i^{lk} = 1$: if $f_i^l < f_i^k$, then $v_i^{lk} = 0$; if $f_i^l = f_i^k$, then $v_i^{lk} = -1$; and if $f_i^l > f_i^k$, then r_{lk} is determined as

$$\begin{aligned} r_{lk} &= 1, \quad v_i^{lk} \geq 0 \quad i \in \{1, 2, \ldots, m\} \quad \text{and} \quad \sum_{i=1}^{m} v_i^{lk} \neq 0 \\ r_{lk} &= -1, \quad v_i^{lk} \leq 0 \quad i \in \{1, 2, \ldots, m\} \quad \text{and} \quad \sum_{i=1}^{m} v_i^{lk} \neq 0 \\ r_{lk} &= 0, \quad \text{else} \end{aligned} \tag{13}$$

For the matrix $R = [r_{ik}]_{N\cdot N}$ in the l row, if $r_{lk} \geq 0$ (k= $1, 2, \ldots, N$), then l is the first-degree nondominated individual. All of the Pareto-optimal solutions consist of first-degree nondominated individuals.

D. Multi-Objective Genetic Algorithm Process

Multi-objective optimizations are carried out as the following steps:

1) Code the problem to the design space.

2) Generated the original population randomly.

3) Find out the first-degree nondominated solution for each individual.

4) Copy the first-degree nondominated individuals to the Pareto pool.

5) Calculate the fitness of each individual.

6) Process the generic operation (selection, intersection, and mutation) and generate a new population or execute the adaptive operation every N generation.

7) Evaluate each individual of these new populations.

8) Copy the first-degree nondominated individuals to the Pareto pool. Evaluate all individuals in the Pareto pool and only save the first-degree nondominated individuals.

9) Decode the results if the termination condition has been succeeded. Otherwise, go to step 6.

IV. Results and Discussion

A. Static Aeroelastic Analyses

The static aeroelastic solver was developed based on our dynamic aeroelastic solver [19,20], in which the structural modes were employed and the characteristics of aileron buzz and gust responses were analyzed; the static aeroelastic solver still needs to be validated, due to the use of stiffness matrix in the structure.

In 2007, a static aeroelastic experiment was conducted in a Chinese transonic wind tunnel. The experimental model is a wing-body configuration with the rigid body and the flexible wing shown in Fig. 1a, which has a 0.7755 m length of mean aerodynamic chord and a 1.2607 m length of half-span, and 62 pressure measurement points are distributed on the upper and lower wing surfaces in the three spanwise sections of 0.53043, 0.77298, and 1.14538 m, respectively. The experimental angles of attack were taken as −1.5, 0.5, and 2.5 deg; the experimental dynamic pressures were 21.8 and 30 kPa; and the experimental flap deflections were −5, 0 deg. The experimental purposes were to study the static aeroelastic influences with the flap deflections and provide the experimental data for the validation of static aeroelastic solver. The structural stiffness matrix of the flexible wing was obtained from the finite element analyses with MSC Nastran software. The structural grid points on the wing and the control surface are shown in Fig. 1b.

All experimental cases have been calculated with the developed static aeroelastic solver. The agreements between experiments and calculations are fairly good. Figure 2 only gives the comparison of pressure distribution on the span sections of $y = 0.53043$ m; 0.77298 m just cross the flap surface at a Mach number of $M_\infty = 0.6$; dynamic pressure $Q = 30$ kPa; flap deflection of $\beta = -5$; and angles of attack $\alpha = -1.5$, 0.5, and 2.5 deg. Excellent agreement is shown on the wing, flap, and gap.

Another static aeroelastic example is the high-aspect-ratio wing, which will be studied for its static aeroelastic optimization in the next section. For the model shown in Fig. 3a, span sections of A-A, B-B, C-C, and D-D have the same airfoil shape. Because there are no experimental data, only the comparison between rigid and flexible results is given. Figure 3b shows the structural deformation and pressure contours at a cruise Mach number of 0.6 and angle of attack of 2 deg. The structural deformation exhibits mainly in the outer wing, which increases gradually from the root to the tip of the wing. These can also be seen in Fig. 4, in which the comparison of pressure distributions at six span sections is given. Table 1 shows the comparison of aerodynamic coefficients. Compared with the rigid wing, the lift coefficient due to structural deformation reduced about 11%, drag coefficient reduced 3%, ratio of lift to drag reduced 8%, pitching moment coefficient reduced 14%, and the position of pressure center moved forward about 3.5%.

B. Static Aeroelastic Optimization

From the preceding static aeroelastic analyses for the high-aspect-ratio wing, the results show that the structural deformation is small in the inner wing and large in the outer wing. How to optimize the airfoil shapes in the outer wing and how to make the aerodynamic performance of the flexible wing to return to that of the original rigid wing is the purpose of this investigation.

In the optimization process, the airfoil shapes in the inner wing (such as A-A section), the planar shape of the wing, and the structural stiffness matrix are considered to be fixed. We take the airfoil sections of B-B and C-C as optimization configurations, as shown in Fig. 3a. The wing tip airfoil of the D-D section is taken to be the same shapes as the airfoil of the C-C section, and the other wing surface is

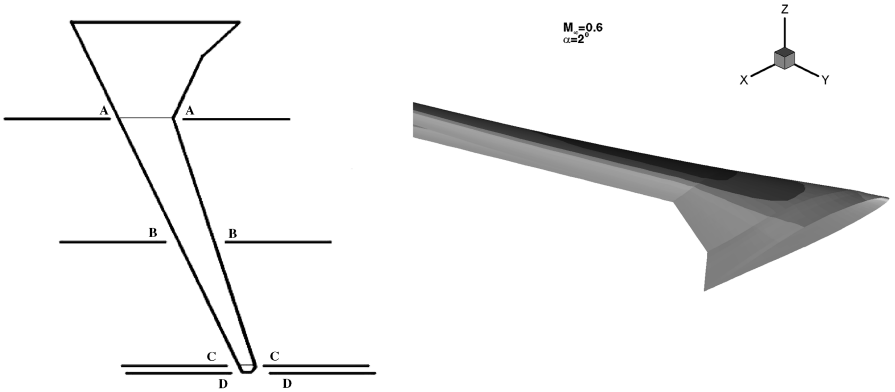

a) Wing model b) Structural deformation

Fig. 3 Illustrations of a) wing model and b) structural deformation.

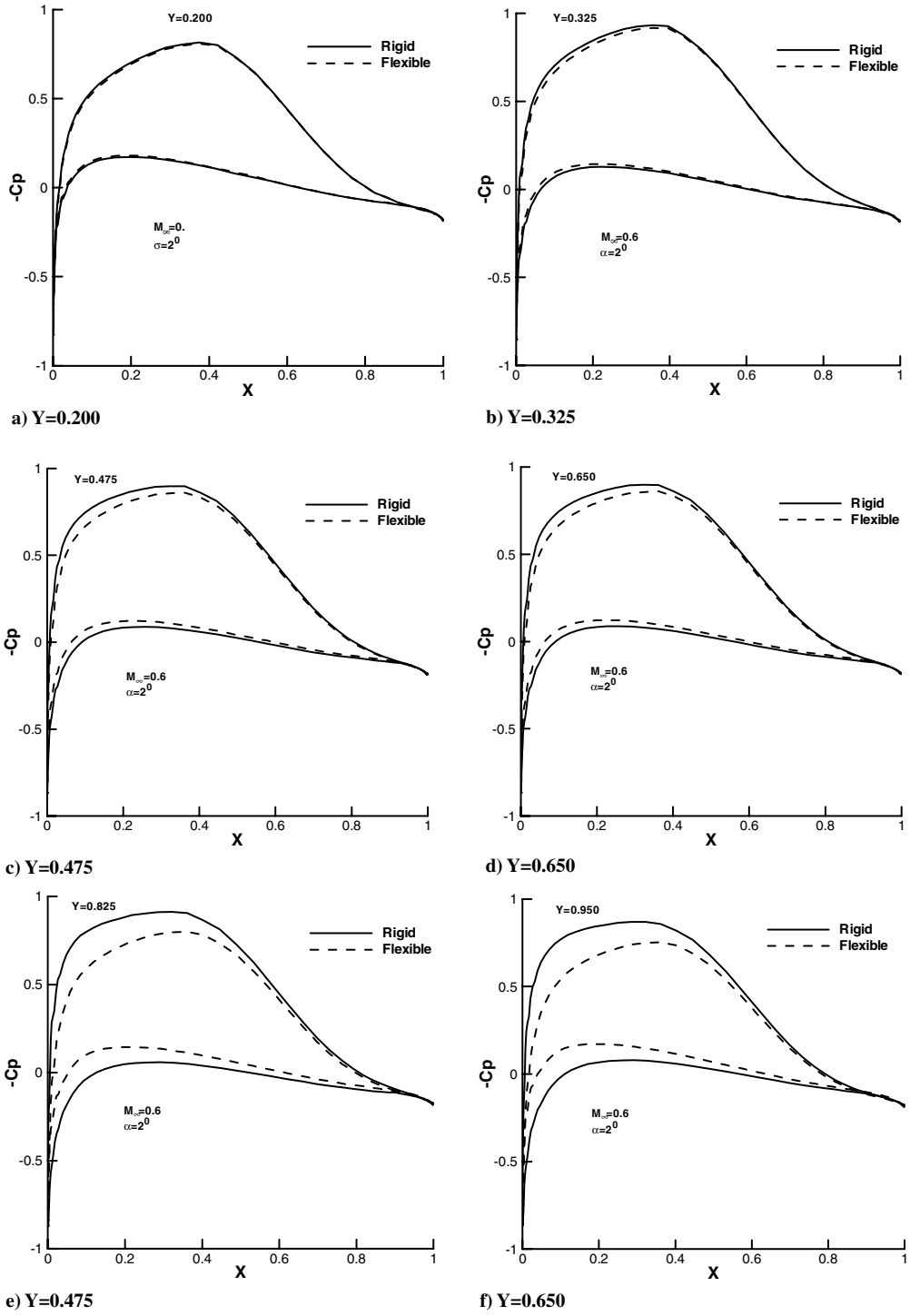

Fig. 4 Span pressure comparison between rigid and flexible wings.

obtained by linear interpolation from the A-A, B-B, and C-C sections. The third-order B-spline curves are used for the parameterization of the B-B and C-C sections. The design variables are the coordinates of control points of the B-spline curve. Each airfoil has 12 control points, and total 24 design variables are required for the optimization.

Table 1 Comparison of aerodynamic coefficients between rigid and static elastic calculations

Wing	C_L	C_D	L/D	C_M	X_{cp}
Rigid	0.3949	0.0208	19.03	−0.2149	0.5436
Flexible	0.3511	0.0201	17.49	−0.1843	0.5244

According to the quadratic polynomial RSM model used in the study, there are 325 unknown parameters that need to be determined. Based on the orthogonal design method (based on the function of $K = (k+1)(k+2)/2$), 500 samples are randomly generated through the perturbation of design variables from the original airfoil parameters. Aerodynamic coefficients of these samples are calculated with the static aeroelastic solver as the database; 325 samples are elicited randomly for the RSM model, and the others are taken as the check samples. For the check samples, R^2 and R_a^2 in Eq. (8) are taken as the evaluation standard. If either the lift coefficient or drag coefficient, R^2 and R_a^2, is larger than 0.99999, it indicates that the RSM model is more precise for the model of the lift and drag coefficients, which can be used to replace the static aeroelastic calculations in the optimization process.

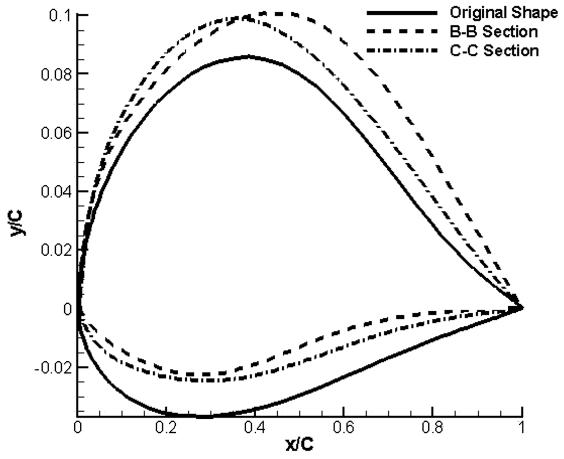

Fig. 5 Optimization airfoils at B-B and C-C sections.

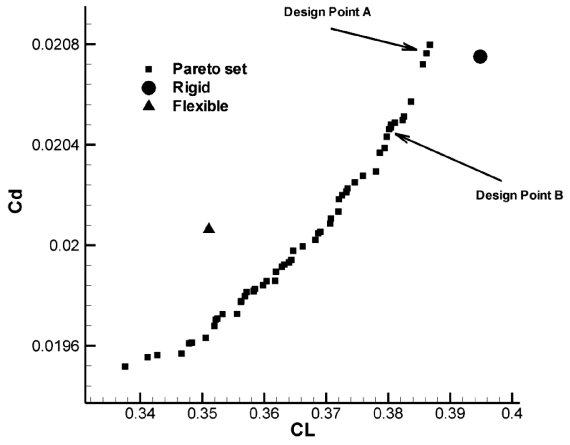

Fig. 6 Pareto-optimal solutions for multi-objective optimization.

In the ARGAs calculation, the population number of each generation is set to be 500 and the maximum generation is 1000. The adaptive cross probabilities are set to $P_{c1} = 0.9$ and $P_{c2} = 0.6$, and the mutation probabilities are set to $P_{m1} = 0.1$ and $P_{m2} = 0.001$.

First, the single-objective optimization is investigated. The objective function is the lift coefficient of C_L to be maximized, and the maximum thickness is greater than that of the original airfoil as the constraint condition. The optimizations of the B-B and C-C sectional airfoils compared with the original airfoil are given in Fig. 5. The aerodynamic performances from the RSM-based ARGAs are $C_L = 0.3957$, $C_D = 0.022946$, and $L/D = 17.618$. Comparing the original static aeroelastic result, the lift coefficient of static aeroelastic optimization improves about 12.7%; slightly larger than that of the rigid wing, however, the drag coefficient also increases about 14.16%.

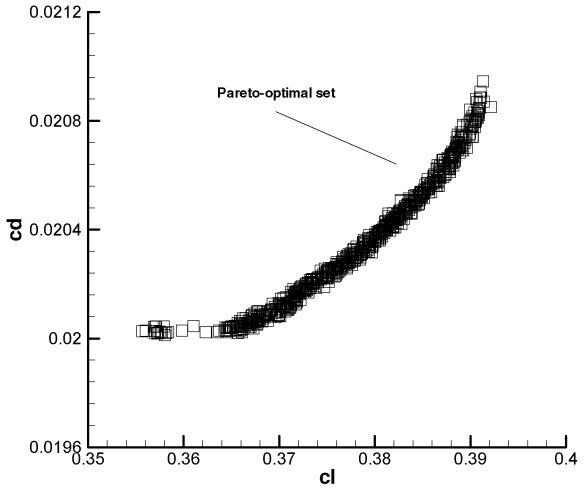

Fig. 8 Pareto-optimal set of 10 time GA optimizations.

Second, the multi-objective optimization is investigated. The objective functions are the maximum of lift coefficient and the minimum of drag coefficient. The Pareto-optimal solutions are given in Fig. 6. In the figure, the black circle and triangular points represent the original rigid solution and the original static aeroelastic solution, respectively. All Pareto-optimal solutions dominate the original static aeroelastic solution but do not dominate the original rigid solution. It means that the optimization can improve the static aeroelastic performance, but is still hard to exceed the performance of the original rigid wing. We further check the design points A and B on the Pareto-optimal solutions. For design point A, its lift coefficient approaches the rigid result, and the drag coefficient nearly equals the rigid solution. For design point B, its lift and drag coefficients are smaller than those of rigid results but larger than those of the original static aeroelastic results. Figure 7 gives the comparison between the optimal airfoils and the original airfoil at sections B-B and C-C. The comparison of the static aeroelastic aerodynamic performances at design points A and B is given in Table 2.

Because the GA optimization is a stochastic search method, the results are dependent on the initial population samples. Because the RSM model is constructed beforehand based on the database of CFD-based static aeroelastic calculations, the RSM-based ARGAs optimization is computationally efficient. The Pareto-optimal solutions of 10 GA operations are given in Fig. 8. The results indicate

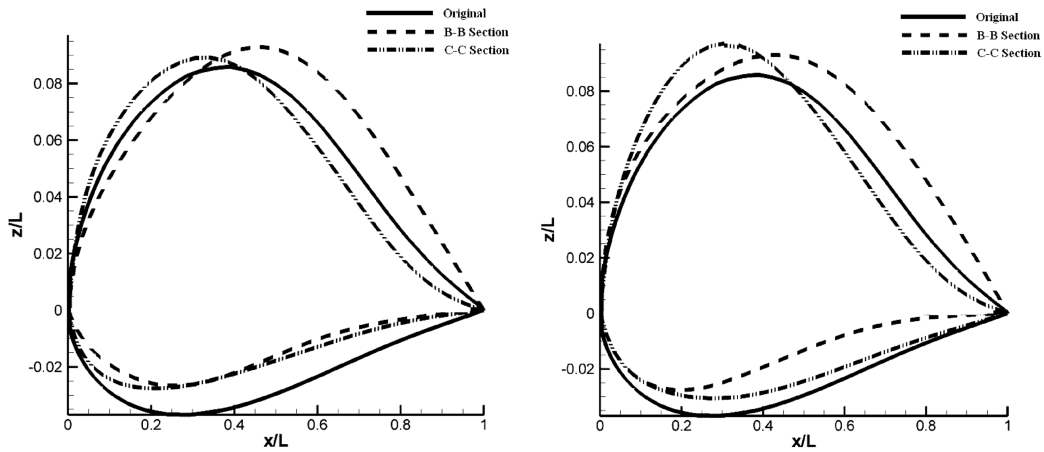

a) Design point A **b) Design point B**

Fig. 7 Comparison of multi-objective optimal airfoils.

Table 2 Comparison of static aeroelastic aerodynamic performance of multi-objective optimization at design points A and B

Design point	C_L	C_D	L/D
A	0.3862	0.02076	18.60
B	0.3802	0.02046	18.58

that the scatter degree of different optimization processes is small and the Pareto-optimal solutions seem insensitive to the initial random samples.

V. Conclusions

Because of too-large time costs, the direct CFD-based fluid/structure multidisciplinary optimization is still difficult to use for aircraft design. In this Note, a high-efficiency static aeroelastic aerodynamic optimization method was developed. CFD-based static aeroelastic calculations were only used for the construction of the response surface model, and the whole optimization process needs very little time, due to the replacement of the direct CFD-based static aeroelastic calculations with the RSM model.

For a high-aspect-ratio wing, single- and multi-objectives static aeroelastic optimizations were investigated in which static aeroelastic aerodynamic performances were calculated with the Reynolds-averaged Navier–Stokes equations coupled with the structural statics equation, the quadratic polynomial function was taken as the RSM model, and the real-coded adaptive-range genetic algorithms was chosen as the optimization method. The results indicate that the static aeroelastic aerodynamic performance can be greatly improved and is insensitive to the choice of initial population samples. The developed method is effective for multidisciplinary optimization.

References

[1] Jameson, A., "Aerodynamic Design Via Control Theory," NASA CR-181749, Nov. 1988.

[2] Deb, K., *Multi-Objective Optimization Using Evolutionary Algorithms*, Wiley, New York, 2001.

[3] Bennett, R. M., and Edwards, J. W., *An Overview of Recent Developments in Computational Aeroelasticity*, AIAA Paper 98-2421, June 1998.

[4] Smith, M. J., Hodges, D. H., and Cesnik, C. E. S., *An Evaluation of Computational Algorithms to Interface Between CFD and CSD Methodologies*, U.S. Air Force Wright Aeronautical Labs., WL-TR-96-3055, Dayton, OH, Nov. 1995.

[5] Jones, W. T., and Samareh-Abolhassani, J., "A grid Generation System for Multidisciplinary Design Optimization," *12th AIAA Computational Fluid Dynamics Conference*, AIAA, Washington D.C., 1995, pp. 474–482.

[6] Batina, J. T., "Unsteady Euler Airfoil Solutions Using Unstructured Dynamic Meshes," *AIAA Journal*, Vol. 28, No. 8, 1990, pp. 1381–1388. doi:10.2514/3.25229

[7] Farhat, C., Degand, C., Koobus, B., and Lesoinne, M., *Improved Method of Spring Analogy for Dynamic Unstructured Fluid Meshes*, AIAA Paper 98-2070, Apr. 1998.

[8] Chen, P. C., and Hill, L. R., *A Three-Dimensional Boundary Element Method for CFD/CSD Grid Interfacing*, AIAA Paper 99-1213, 1999, pp. 88–98.

[9] Guruswamy, G. P., and Obayashi, S., *Use of High-Fidelity Methods in Multidisciplinary Optimization—A Preliminary Study*, AIAA Paper 2002-5638, Sept. 2002.

[10] Martins, J. R. R. A., Alonso, J. J., and Reuther, J. J., *High-Fidelity Aero-Structural Design Optimization of a Supersonic Business Jet*, AIAA Paper 2002-1483, Apr. 2000.

[11] Martins, J. R. R. A., Alonso, J. J., and Reuther, J. J., *Complete Configuration Aero-Structural Optimization Using a Coupled Sensitivity Analysis Method*, AIAA Paper 2002-5402, Sept. 2002.

[12] Martins, J. R. R. A., Alonso, J. J., and Reuther, J. J., "Aero-Structural Wing Design Optimization Using High-Fidelity Sensitivity Analysis," *CEAS Conference on Multidisciplinary Aircraft Design Optimization*, Cologne, Germany, June 2001, pp. 211–226.

[13] Reuther, J. J., Alonso, J. J., Martins, J. R. R. A., and Smith, S. C., *A Coupled Aero-Structural Optimization Method for Complete Aircraft Configurations*, AIAA Paper 99-0187, Jan. 1999.

[14] Obayashi, S., and Guruswamy, G. P., "Convergence Acceleration of a Navier–Stokes Solver for Efficient Static Aeroelastic Computations," *AIAA Journal*, Vol. 33, No. 6, 1995, pp. 1134–1141. doi:10.2514/3.12533

[15] Yang, G. W., Kondo, M., and Obayashi, S., "Multiblock Navier–Stokes Solver for Wing/Fuselage Transport Aircraft," *JSME International Journal, Series B (Fluids and Thermal Engineering)*, Vol. 45, No. 1, 2002, pp. 85–90. doi:10.1299/jsmeb.45.85

[16] Madsen, J. I., Shyy, W., and Haftka, R. T., "Response Surface Technique for Diffuser Shape Optimization," *AIAA Journal*, Vol. 38, No. 9, 2000, pp. 1512–1518. doi:10.2514/2.1160

[17] Arakawa, M., and Hagiwara, I., "Development of Adaptive Real Range Genetic Algorithms," *JSME International Journal, Series C*, Vol. 41, No. 4, 1998, pp. 969–977.

[18] Goldberg, D. E., *Genetic Algorithm in Search, Optimization and Machine Learning*, Addison Wesley, Reading, MA, 1989.

[19] Yang, G. W., Obayashi, S., and Nakamichi, J., "Aileron Buzz Simulation Using an Implicit Multiblock Aeroelastic Solver," *Journal of Aircraft*, Vol. 40, No. 3, 2003, pp. 580–589. doi:10.2514/2.3134

[20] Yang, G. W., and Obayashi, S., "Numerical Analyses of Discrete Gust Response for an Aircraft," *Journal of Aircraft*, Vol. 41, No. 6, 2004, pp. 1353–1359. doi:10.2514/1.2531